Estuarine and Tidal Currents in the Broughton Archipelago

M.G.G. Foreman[1*], D.J. Stucchi[1], Y. Zhang[2] and A.M. Baptista[2]

[1]*Institute of Ocean Sciences, Fisheries and Oceans Canada, Sidney BC V8L 4B2*
[2]*Oregon Health and Science University, Beaverton, OR U.S.A.*

[Orginal manuscript received 2 August 2005; in revised form 11 October 2005]

ABSTRACT *Current meter observations, Conductivity-Temperature-Depth (CTD) profiles, and river discharges are combined with two numerical models to understand better the estuarine and tidal circulation in the Broughton Archipelago, a complex region of islands, channels, and fiords that has become a primary location for salmon farms in British Columbia. Though tidal currents are strong in many sub-regions, the primary transport mechanisms in the archipelago are the estuarine flows resulting from river and glacial runoff, and the near-surface currents that arise from strong winds. The harmonic finite element model, TIDE3D, is shown to reproduce the barotropic tidal currents with reasonable accuracy, but unlike other regions of the British Columbia coast where an extensive archive of historical observations has permitted a diagnostic calculation of average seasonal flows, sparse and noisy CTD observations did not allow a similar computation here. In order to simulate these background flows, the prognostic finite volume model, ELCIRC, was initialized with a smoothed version of these same historical temperature and salinity fields and forced with tides and river discharge. Though the near-surface flows were reproduced with acceptable accuracy, the estuarine and tidal flows at depth were found to be much too weak as a result of numerical dissipation arising from the Eulerian-Lagrangian time stepping. Nevertheless, ELCIRC did confirm current observations suggesting that the bottom estuarine flow in Knight Inlet actually comes from Queen Charlotte Strait via the "back-door" of Fife Sound and Tribune Passage. Consistent with anecdotal evidence, ELCIRC also showed that the surface estuarine flow coming down Knight Inlet bifurcates with part going down Tribune Channel and Fife Sound and part continuing down Knight Inlet. The relevance of these background flows for aquaculture issues, such as oxygen renewal and the transport of sea lice and viruses, is discussed.*

RÉSUMÉ *[Traduit par la rédaction] Des observations par courantomètres, des profils conductivité-température-profondeur (CTP) et des débits de rivières sont combinés avec deux modèles numériques pour mieux comprendre la circulation estuarienne et de marée dans l'archipel Broughton, une région complexe d'îles, de détroits et de fjords qui est devenue une importante région de pisciculture de saumons en Colombie-Britannique. Même si les courants de marée sont forts dans plusieurs sous-régions, les principaux mécanismes de transport dans l'archipel sont les débits estuariens dus à l'eau des rivières et des glaciers et les courants superficiels engendrés par le vent. Le modèle harmonique aux éléments finis, TIDE3D, reproduit les courants de marée barotropes avec une précision raisonnable mais, contrairement à d'autres régions de la côte de la Colombie-Britannique pour lesquelles une grande quantité de données historiques archivées a permis un calcul diagnostique des débits saisonniers moyens, les observations CTP éparses et bruitées n'ont pas permis de faire le même calcul ici. Pour simuler ces débits de base, le modèle pronostique aux volumes finis, ELCIRC, a été initialisé avec une version lissée de ces mêmes champs historiques de température et de salinité et forcé avec les marées et le débit des rivières. Bien que les débits superficiels aient été reproduits avec une précision acceptable, les débits estuariens et de marée en profondeur se sont avérés beaucoup trop faibles sous l'effet de la dissipation numérique découlant du schéma eulérien-lagrangien de pas de temps. Néanmoins, l'ELCIRC a confirmé les observations de courants, ce qui suggère que le débit au fond de l'estuaire dans l'anse Knight provient en fait du détroit de la Reine-Charlotte par le biais du détroit Fife et du passage Tribune. En accord avec des indications anecdotiques, l'ELCIRC a aussi montré que le courant estuarien de surface en provenance de l' anse Knight bifurque pour en partie passer dans le chenal Tribune et le détroit Fife et en partie continuer dans l' anse Knight. On discute de la pertinence de ces courants de base dans les questions d'aquaculture telles que le renouvellement de l'oxygène et le transport du pou de poisson et des virus.*

1 Introduction

The Broughton Archipelago (Figs 1 and 2) is a complex network of islands, channels, and fiords lying off the mainland of British Columbia, approximately 300 km north-west of Vancouver. In addition to river and glacial runoff that enters from the nearby mountainous terrain, circulation within the archipelago is also forced by: winds and the strong tidal and estuarine flows in Johnstone Strait (Thomson and Huggett, 1980; hereinafter TH80); the deep channel leading south-eastward to the Strait of Georgia; and in Queen Charlotte Strait, the much wider westward access to Queen Charlotte Sound and the Pacific Ocean. Though relatively remote in terms of settlements and accessibility, the region has become a

*Corresponding author's e-mail: foremanm@pac.dfo-mpo.gc.ca

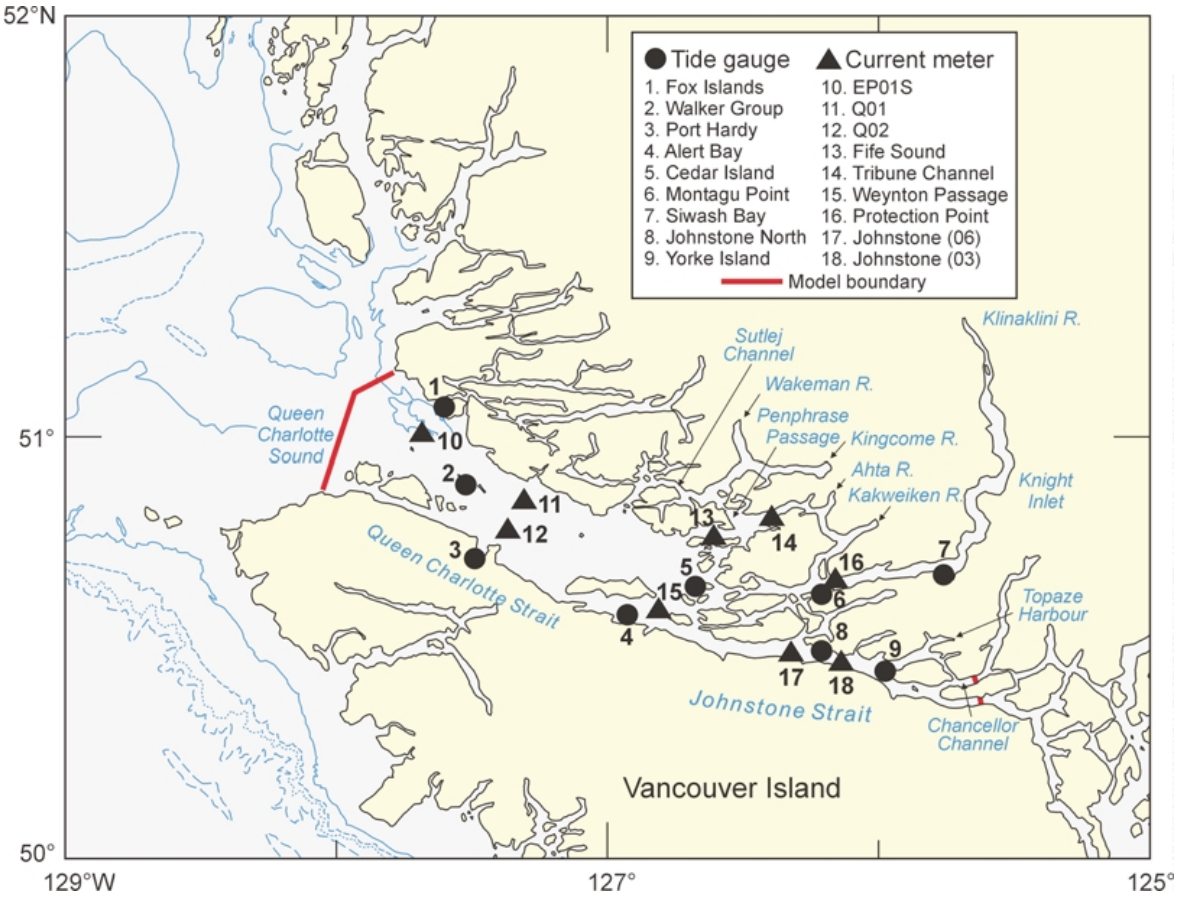

Fig. 1 Map of the Broughton Archipelago region showing tide gauge and current meter observation sites for evaluating model performance. Names of numbered sites are referred to in Tables 1–3.

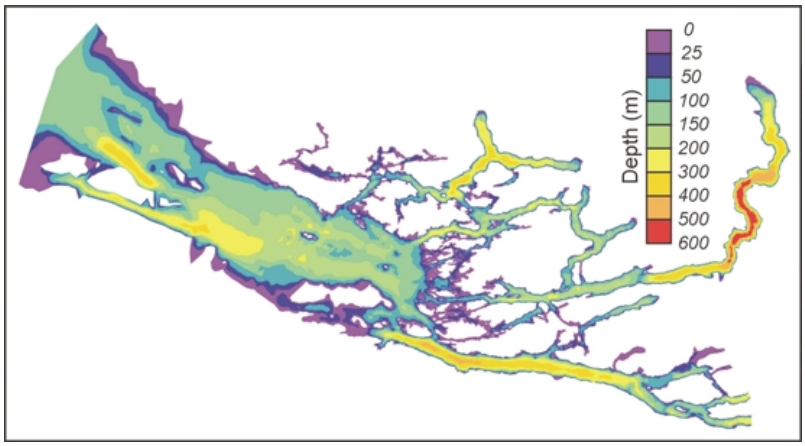

Fig. 2 Bathymetry (m) of the region.

primary location for salmon farms in British Columbia. Of the approximately 131 finfish farm sites in the province, about thirty are located in the archipelago. In 2003, a total of 70,600 tonnes of farmed salmon were harvested (Statistics Canada, 2005), most of which was shipped to markets in the United States.

Though Knight Inlet (Figs 1 and 2) has been a widely studied natural laboratory (Freeland and Farmer, 1980; Farmer and Freeland, 1983) for the internal tides that are generated at its inner sill (Farmer and Smith, 1980a, 1980b; Webb and Pond, 1986; Marsden and Greenwood, 1994), until recently there had been very few physical observations taken in the rest of the Broughton Archipelago. As a result, the circulation was largely unknown. Circulation is a critical factor for fish farms, determining not only the availability of dissolved oxygen throughout the region but also the dispersal patterns of

both solid and soluble wastes and the subsequent recovery time for benthic communities. A detailed knowledge of circulation patterns can thus be extremely helpful in selecting aquaculture sites that minimize environmental impacts, do not stress the local carrying capacity, and avoid regular detrimental effects such as harmful algal blooms. In 2002, a collaborative project between Fisheries and Oceans Canada and Stolt Sea Farms Inc. was initiated to augment the sparse physical oceanographic information in the Broughton Archipelago with a combination of field observations and numerical circulation modelling. This paper describes some results of that study.

Pickard and Rogers (1959) were the first to make current observations in Knight Inlet. In times of relatively calm winds near the inner sill, they observed net estuarine flows of approximately ±20 cm s^{-1} near the surface and at about 60-m depth. Using an extensive array of moored and profiling currents meters, Baker and Pond (1995) found a high correlation between winds and surface flows during two month-long periods in 1988 and 1989. After removing wind and tidal influences from these measurements, near-surface down-inlet average flows during a period of average discharge in late June 1989 were seen to be as large as 20 cm s^{-1} while the compensating up-inlet flows at depth were much smaller and thought to be non-representative because of cross-channel variations. Using their own and previously collected Conductivity-Temperature-Depth (CTD) data, Baker and Pond (1995) also showed that, depending on the magnitude of the discharge from the Klinaklini River, down-inlet surface slopes could be as high as 2×10^{-6} m m^{-1} and thus dynamic heights at the head of the inlet could be as much as 20 cm higher than at the mouth.

Stacey et al. (1995) used a laterally integrated, two-dimensional model to simulate successfully the mean, tidal and wind circulation during the same two measurement periods studied by Baker and Pond (1995). However, this success was found to be dependent on augmenting the standard Mellor-Yamada vertical diffusion coefficients (Mellor and Yamada, 1982) by an extra term that could be interpreted as representing the mixing caused by breaking internal waves.

TH80 used tide, current, and water property data to describe the tidal (barotropic and baroclinic) and estuarine flows in Johnstone Strait. They demonstrated that internal tides were generated at a shallow sill near the eastern end of the channel and found westward mean flows with magnitudes up to 30 cm s^{-1} in the upper 100 m of the channel and eastward mean flows with magnitudes up to 20 cm s^{-1} in the lower 200 m. A relatively high (>4.5 mL L^{-1}) and near-uniform distribution of dissolved oxygen observed throughout the year suggested vigorous tidal pumping and turbulent mixing along the entire length of the channel. This was confirmed by analyses that computed M_2 along-channel current amplitudes as large as 50 cm s^{-1}.

To augment current observations and facilitate our understanding of the numerous environmental issues associated with the presence of both natural and farmed salmon in the Broughton Archipelago, the unstructured grid methods TIDE3D and ELCIRC have been used to develop three-dimensional (3D) ocean circulation models for the region. TIDE3D is the harmonic finite element method developed by Walters (1988, 1992) that has been applied successfully to several shelf regions around the world including some in British Columbia (Walters et al., 2001; Foreman et al., 1995; Foreman and Thomson, 1997). It provides an efficient and accurate methodology for computing 3D barotropic tidal heights and currents, diagnostic buoyancy currents arising from a specified density field, and steady-state wind-driven currents arising from a periodic or time-invariant wind field. However, because both the density and wind fields are restricted in their temporal variations (i.e., they must be periodic), TIDE3D cannot be used to simulate internal tides or transient responses to irregular forcing such as would arise from storms and variable river discharge. Nevertheless, it is a useful tool that will be employed here to provide benchmark tidal solutions for evaluating the more sophisticated model, ELCIRC.

ELCIRC is a finite volume/finite difference method that was originally developed for simulations of the Columbia River estuary and plume (Zhang et al., 2004; Baptista et al., 2005) but has recently been applied to the northern British Columbia shelf (Robinson et al., 2005), the Guadiana estuary in Portugal (Anabela Oliveira, personal communication, 2004), and the Red Sea (Cheryl Ann Blain, personal communication, 2004). ELCIRC solves 3D hydrodynamic equations for velocity and surface elevation and 3D transport/diffusion equations for salinity and temperature in the presence of turbulent mixing. As with diagnostic finite element methods such as TIDE3D and prognostic finite element models such as QUODDY (Lynch et al., 1996), ELCIRC allows the flexibility of a variable grid to provide a better representation of complicated regions such as the coastline and bathymetry found in the Broughton Archipelago. However, it has additional attributes such as: a) Eulerian-Lagrangian time stepping, b) local volume conservation, c) a choice of several high and low order mixing schemes, d) a horizontal grid that can be a combination of triangles and/or quadrilaterals, and e) level rather than terrain-following coordinates in the vertical, that should make it more accurate, efficient, and computationally robust than many prognostic finite element techniques. ELCIRC can be forced with any combination of tides, winds, river runoff, and surface heating, and in this application will be initialized with salinity and temperature fields that were constructed from historical observations. A more complete description of the model techniques, recommended parameter values, and performance in a series of test problems and real applications can be found in Zhang et al. (2004), Baptista et al. (2005), and the Center for Coastal and Land-Margin Research (2004).

This paper is organized as follows. In Section 2, the model setup, tidal and river discharge forcing, and the calculation of a spring salinity and temperature climatology are briefly

described. In Section 3, ELCIRC runs simulating the average spring circulation that arises from river discharge and estuarine forcing are carried out. Tides are also included in these runs and the associated time series of tidal heights and tidal and mean currents are analysed and compared with historical tide gauge and current meter observations and TIDE3D results. Finally, in the last section, the results are summarized and future work is outlined.

2 Model setup and forcing

The triangular grid for the model (Fig. 3) has 21,560 nodes, 37,543 triangles, and triangle sides that vary in length from approximately 6 km in Queen Charlotte Strait to less than 50 m in some of the narrow channels. The grid was constructed with the software package GRIDGEN and its predecessor TRIGRID (Henry and Walters, 1993). Although the triangles produced by these packages do not, in general, conform with the orthogonality constraint imposed by UNTRIM (Casulli and Walters, 2000), a predecessor of ELCIRC, they have been checked with the "equilateralness" option in TRIGRID and modified to eliminate those with angles larger than 90°. Experimentation has shown that triangles having this property seem to avoid the instability and/or energy trapping behaviour that more poorly shaped triangles sometimes exhibit with ELCIRC. Though ELCIRC can also use quadrilateral elements, and there is some evidence to suggest that these elements may be more accurate than triangles, quadrilaterals have not been employed here in order to permit comparisons with TIDE3D, which can only use triangles. Though TIDE3D does not have an orthogonality constraint, its accuracy does deteriorate for triangular elements having large obtuse angles. However, the grid modifications described above mean that this is not an issue here.

Model bathymetry was taken from Canadian Hydrographic Service charts and, for the ELCIRC simulations, it was smoothed so that within each triangle, $\Delta h/h < 1.0$ (where h is the average depth and Δh is the maximum minus minimum depth), a criterion similar to that recommended by Mellor et al. (1994) for the Princeton Ocean Model (POM) and by Hannah and Wright (1995) for QUODDY. Such smoothing is not required by TIDE3D, because the baroclinic pressure gradients are specified externally, and might also be expected to be unnecessary for Z-coordinate models like ELCIRC. However, spurious flows similar to those described by Haney (1991) for sigma-coordinate models do seem to arise because of inconsistencies among the various types of depths (e.g., mid-side, nodal, element) that are used in the ELCIRC calculations. Lower values of $\Delta h/h$, similar to those employed in sigma-coordinate models like POM and QUODDY, severely decreased the mid-channel depths in Knight Inlet and Johnstone Strait and would be expected to affect the barotropic wave propagation speed. Experimentation showed that a value of 1.0 maintained a reasonable representation of the depths in these regions and limited the spurious flow magnitudes to less than 1 cm s^{-1}. So this choice was viewed as a tolerable compromise. The smoothing was done in a manner such that volume was approximately conserved in each 3D triangular prism.

As ELCIRC uses a combination of Eulerian-Lagrangian and implicit time stepping, it does not have to satisfy the usual Courant-Friedrich-Lévy (CFL) constraint for numerical stability. In particular this means that the time steps can be much larger than with conventional methods, and the overall computational run time can be much smaller. However, accuracy does deteriorate with larger time steps and noisy flow patterns have been observed (Baptista et al., 2005) when the time step associated with the baroclinic Courant condition, $\Delta t \leq \Delta x/(g'h)^{1/2}$ where g' is reduced gravity, is exceeded. Applying this baroclinic criterion to our model grid spacing and climatological temperature and salinity values, Δt was chosen to be four minutes. Trial and error tests with other time steps demonstrated that the model results did not improve significantly with lower values. The quadratic bottom friction coefficient was taken to be 0.003 and, as recommended by Zhang et al. (2004), the generic length scale (GLS) closure model proposed by Umlauf and Burchard (2003) was chosen for the turbulent mixing parametrization. Thirty-six levels varying in thickness from 100 m at depths greater than 420 m to 1 m at the surface were used for the vertical discretization in ELCIRC, and twenty-one equally-spaced sigma-surfaces were used in TIDE3D.

As with the ELCIRC simulations, the bottom friction coefficient for TIDE3D was taken to be 0.003. However, the vertical viscosity parametrization in TIDE3D assumes a much simpler formulation than the higher order closure choices available in ELCIRC. In this case, the vertical viscosity was assumed to be proportional to the root mean square bottom velocity (as described in Foreman et al. (1995)) with the associated coefficient taken to be 0.1 m^2 s^{-1}.

Given the mountainous terrain surrounding most of the channels in the archipelago and the fact that the only Environment Canada weather stations in the region are in either Queen Charlotte or Johnstone straits, the accurate specification of wind forcing for the circulation model posed a considerable challenge. A high resolution regional atmospheric model would be a great asset, but unfortunately none exists. Consequently, wind stress has been omitted from the present suite of model forcing but future work is planned to explore the importance of the wind through the acquisition of more wind measurements and the testing of interpolation techniques that, for example, always make the wind direction along-channel.

With the exception of the Klinaklini River (Fig. 1), all of the major rivers flowing into the archipelago are ungauged. Consequently, the freshwater input at the mouths of lesser rivers was simulated by specifying discharges proportional to the ratio of their watershed area relative to that of the Klinaklini. Consistent with the hydrographs (HYDAT CD-ROM, 1999) shown in Fig. 4, an average spring (April – June) discharge of 400 m^3 s^{-1} was imposed for the Klinaklini River. Discharges for the Kingcome, Wakeman, Kakweiken, and Ahta rivers were assumed to follow the same annual average

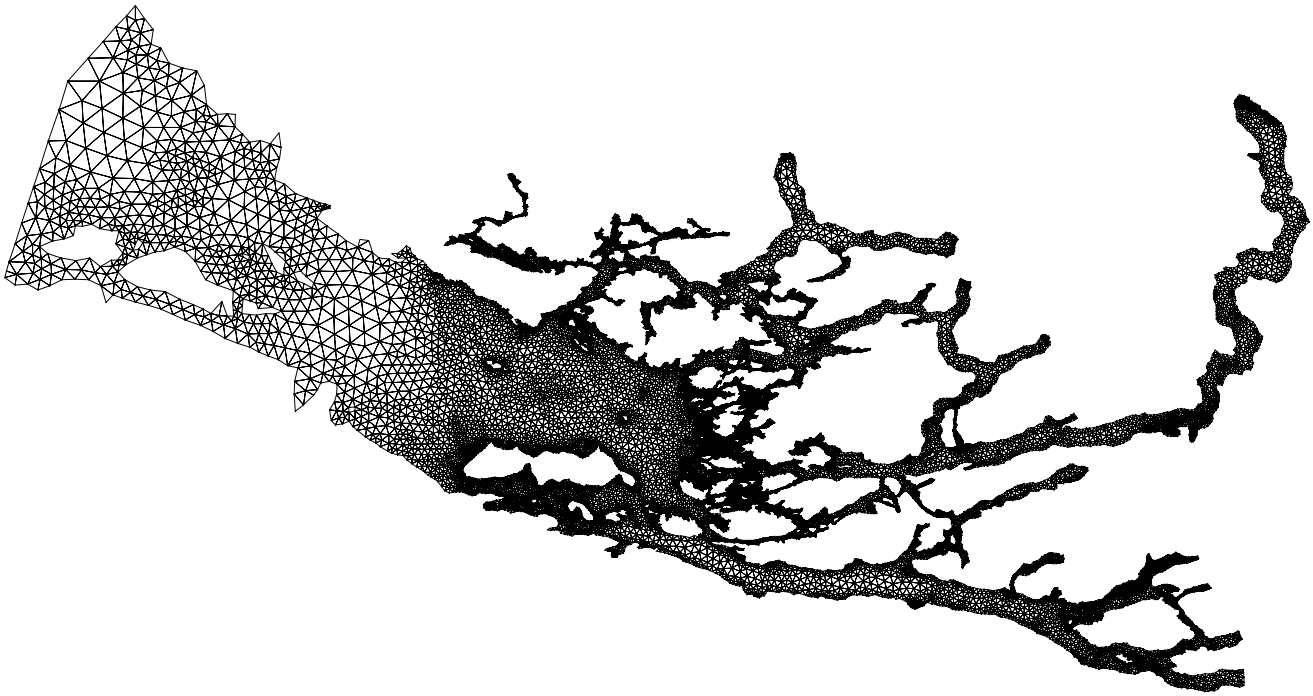

Fig. 3 Triangular grid used in the model calculations.

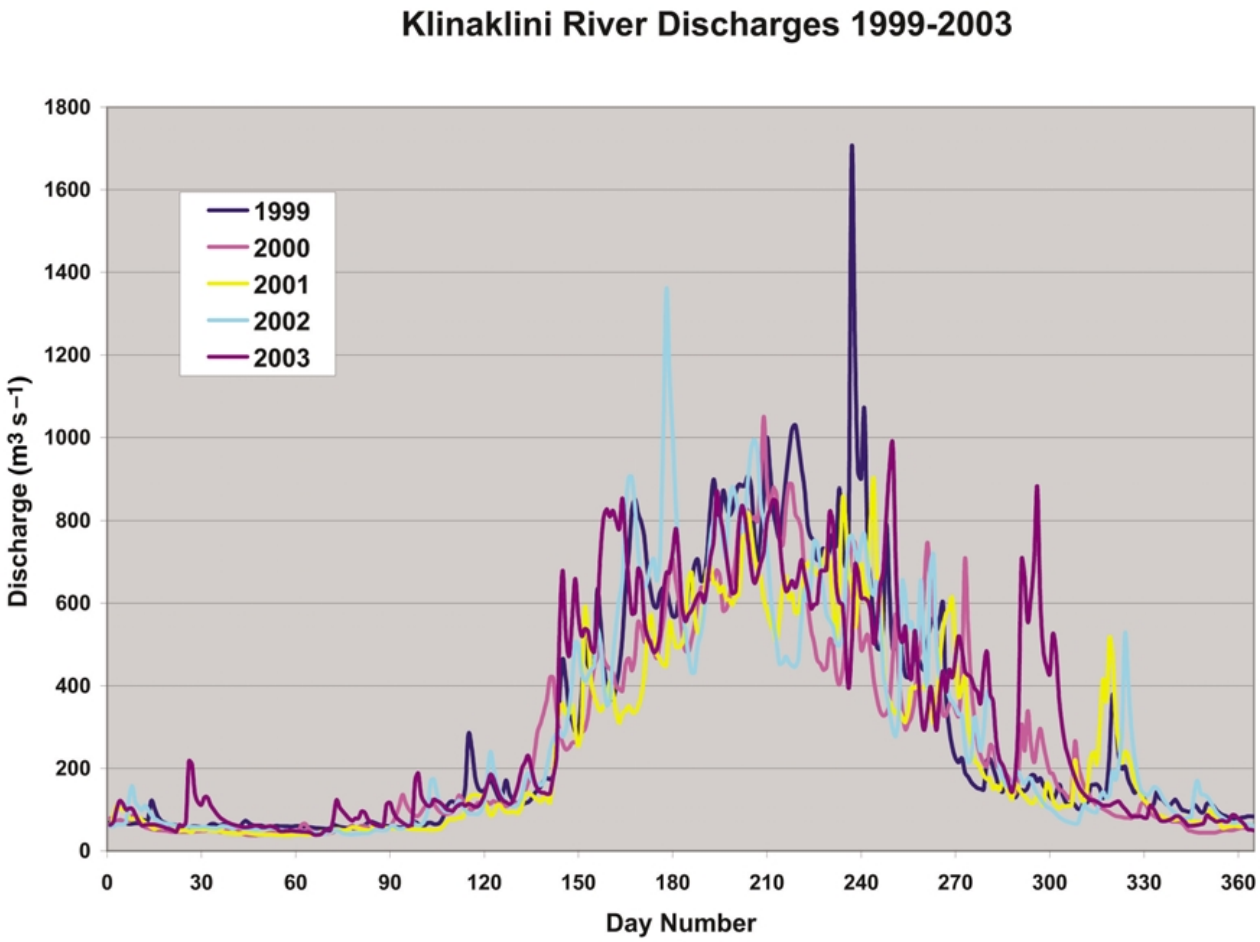

Fig. 4 Klinaklini River discharges ($m^3\ s^{-1}$) for 1999–2003.

variation and assigned values consistent with their approximate watershed areas relative to that of the Klinaklini River; namely 25%, 20%, 10%, and 5% respectively. Temperature and salinity values for these discharges were taken from the surface observations at the CTD station (Fig. 5) closest to each river mouth. A surface heat exchange was imposed indirectly by nudging the surface water temperatures back to their spring climatological values, similar to the procedure adopted in Di Lorenzo et al. (2005). The e-folding scale for this restoration was taken to be five days.

The locations of all historical spring (April – June) CTD sites are shown in Fig. 5 and span the time period from 1951 to 2003. Bad data were eliminated by plotting all profiles and discarding those lying beyond two standard deviations of the mean. Interpolation to the 3D model grid was initially done using a Kriging method within SURFER (Golden Software, 2004) and final smoothing was performed with an irregular-grid diffusion solver. Figure 6 shows the resultant surface salinity and temperature fields. Notice that although the salinities generally have higher values seaward, the temperatures have a noisier pattern that reflects the sparsity of observations and the associated inconsistencies arising from short- (tidal) and long-term (interannual) variability. (Similar plots at other depths were generally noisier than at the surface.) Using the 3D density field consistent with these 3D temperatures and salinities to force a diagnostic TIDE3D calculation analogous to that described in Foreman and Thomson (1997) produced unacceptably noisy elevation and velocity fields. Nevertheless, the same fields were used as initial conditions for the ELCIRC simulations wherein model dynamics, river discharge, and surface heat flux will provide smoothing and remove the inconsistencies.

Although only the results from tidal constituents M_2 and K_1 will be reported here, the four constituents M_2, S_2, K_1, and O_1 were included in all TIDE3D and ELCIRC simulations. This was done to ensure that the major non-linear interactions, primarily via quadratic bottom friction and advection, would be approximately correct. Though the overtides M_4 and MS_4 were generated by ELCIRC and found to be relatively large in regions such as eastern Queen Charlotte Strait and parts of Knight Inlet where Stacey et al. (1995) also found them to be important, they will not be described here. At Alert Bay, M_2, S_2, K_1, and O_1 account for 72% of the tidal height range in the diurnal and semi-diurnal frequency bands. Including the additional constituents N_2, P_1, K_2, and Q_1 would increase the explained tidal content to about 89%. Though this inclusion is easily done for TIDE3D and could be incorporated into future ELCIRC production runs, for the validation studies described here such an inclusion and subsequent analysis would require a run of several months to allow adequate separation of nearby frequencies (Foreman and Henry, 1989). This is beyond our present computing capacity and was not done. Boundary conditions for the tidal and mean components of the circulation model are zero flow normal to the coast and specified elevations along the open sea. Tidal elevation forcing along the Johnstone Strait and Queen Charlotte Strait boundaries of the grid were respectively approximated using tide gauge harmonics from Knox Bay taken from the Canadian Hydrographic Service Blue Book (Fred Stephenson, personal communication, 2004), and larger area model results from either Foreman et al. (1993) or Foreman et al. (2004).

3 Model validation

The primary objective of the model was to use sparse historical temperature and salinity observations, a surface heat exchange, discharge from the Klinaklini River, estimated discharge from Wakeman, Kingcome, Ahta, and Kakweiken rivers, and estuarine flows in Johnstone Strait and Chancellor Channel, to compute a buoyancy circulation that is consistent with available current observations. The Johnstone/Chancellor forcing proved to be somewhat problematic. The Eulerian-Lagrangian treatment of the material derivatives for temperature, salinity, and velocity in ELCIRC means that, whereas the specification of inflow boundary conditions is relatively straightforward, outflow boundaries are not. Specifically, the D/Dt terms in the momentum equations at time t_0 are approximated by velocity values from time $t_0 - \Delta t$ along the backward characteristics. This means that outflow boundaries are forced from inside the model domain while inflow boundaries are forced by the boundary condition. Specifying conditions that would allow both inflow and outflow at the same boundary (e.g., in each Johnstone Strait and Chancellor Channel) was therefore very difficult. On the other hand, experimentation revealed that an estuarine flow is set up relatively easily in the channels downstream of the five river mouths through the specification of fixed volume transports having temperature and salinity values that are consistent with climatology. Given this success and the difficulty of specifying "ready-made" estuarine flows, a pseudo river discharge was established in Topaze Harbour (Fig. 1) with a volume transport of 30,000 $m^3 s^{-1}$, the westward surface estuarine flow estimated by TH80 across a transect that included the Johnstone mooring J03, shown as site 18 in Fig. 1. No discharge was specified along either the Johnstone Strait or Chancellor Channel boundaries under the assumption that the Topaze Harbour discharge would create estuarine currents with the eastward portion of the bottom flow exiting through these boundaries. Though this pseudo discharge caused somewhat complicated flows near the confluence of Chancellor Channel and Johnstone Strait, it will be seen that an estuarine flow does develop further westward in Johnstone Strait.

Tidal forcing for both TIDE3D and ELCIRC was imposed via elevation-specified boundary conditions. ELCIRC was run for fifty days with the boundary tidal forcing ramped up from zero over the first two days. Elevation, velocity, temperature and salinity values were stored every hour at all nodes and specific depths throughout the simulation and a harmonic analysis was performed over the last ten days to extract average fields and tidal energy at constituent frequencies. A low-pass moving average filter was also employed to produce time series of the subtidal salinity, temperature, and

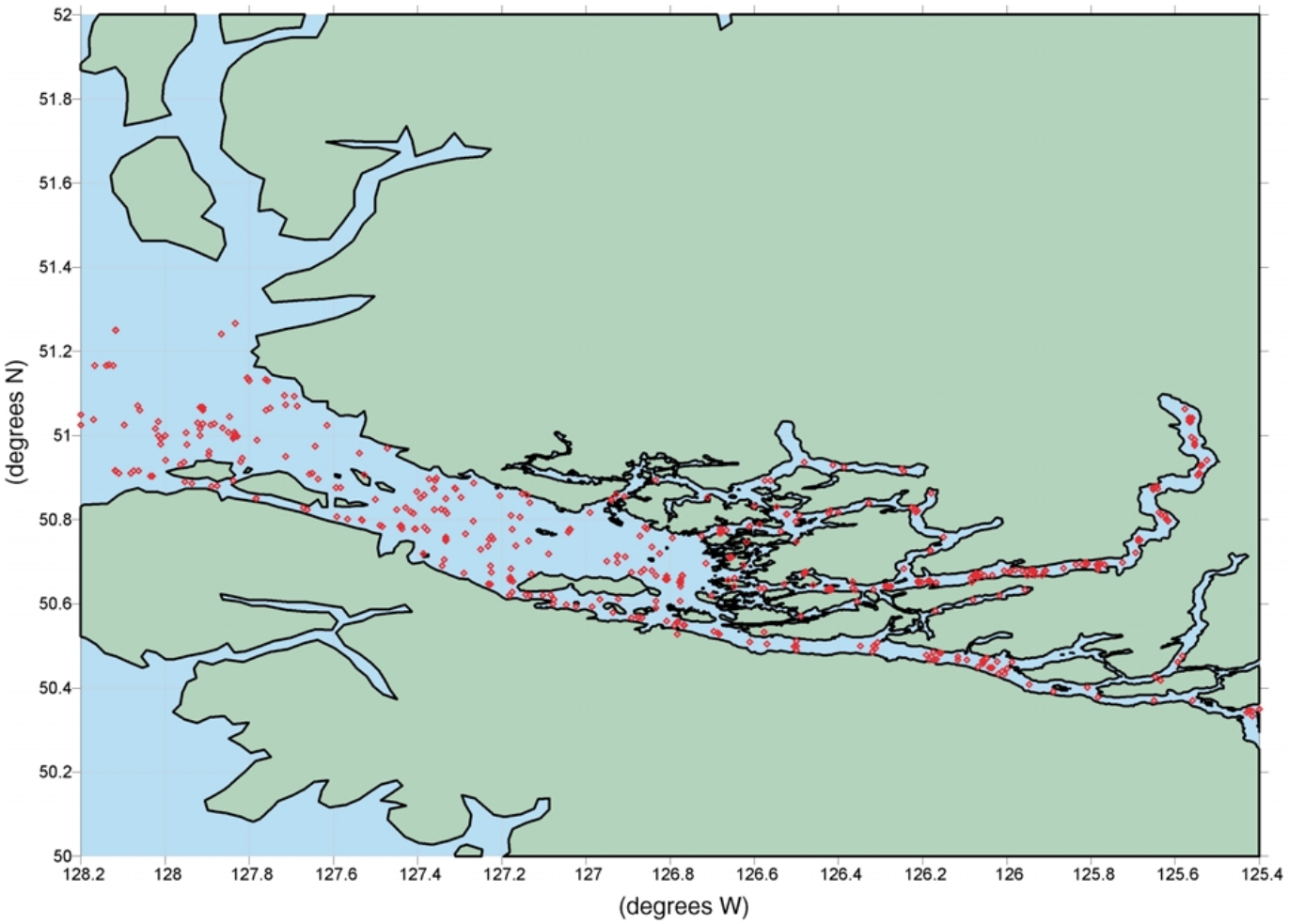

Fig. 5 Location of historical spring salinity and temperature observations within the study region.

flow fields. Comparisons of model results with elevation and current amplitudes and phases computed at the tide gauge and current meter locations shown in Fig. 1 will be discussed later. Elevation differences are calculated as distances, D, in the complex plane; that is,

$$D=\{(A_o\cos g_o-A_m\cos g_m)^2+(A_o\sin g_o-A_m\sin g_m)^2\}^{1/2}, \quad (1)$$

where A_o, A_m, g_o, and g_m are the observed and modelled amplitudes and phases, respectively.

Figure 7 shows the 4-m and 80-m low-pass filtered salinities and flows at day 50 of the ELCIRC simulation while Table 1 compares velocity profiles at nodes closest to current meter sites 10–18 in Fig. 1 with observations at these same sites. Figure 7a shows a near-surface estuarine flow that would be expected from a river discharge entering at the heads of most of the inlets within the archipelago. These flows are basically seaward with magnitudes in each of the various fiords roughly proportional to freshwater input at the head. The steady-state elevation (not shown) at the head of Knight Inlet is approximately 18 cm above that at the mouth, in reasonable agreement with the Baker and Pond (1995) estimates. This elevation gradient drives a seaward near-surface flow that bifurcates at the entrance to Tribune Channel, consistent with qualitative observations (Brent Hargreaves, personal communication, 2004). Some of the seaward flow continues directly westward to Queen Charlotte Strait and some moves northward into Tribune Channel and then westward through Fife Sound before reaching Queen Charlotte Strait. This is consistent with our current meter observations in Fife Sound and Tribune Channel. Westward flows are also seen in Johnstone Strait, from the pseudo river discharges at the south-eastern boundary, and in Sutlej Channel from the discharges of the Kingcome and Wakeman rivers. Noisy patterns that perhaps suggest the need for either further grid refinement or a smaller time step are evident in a few regions such as near the mouth of Knight Inlet and near some small islands in eastern Queen Charlotte Strait. A few eddies, both north and west of Weynton Passage and perhaps in Penphrase Passage (where the eastern link is, at best, weak), are visible in the 4-m flow pattern. As they are also present in the TIDE3D residual flows (not shown), they are likely due to tidal rectification.

The bifurcation of Knight Inlet near-surface flows into Tribune Channel seems to be determined by the relative

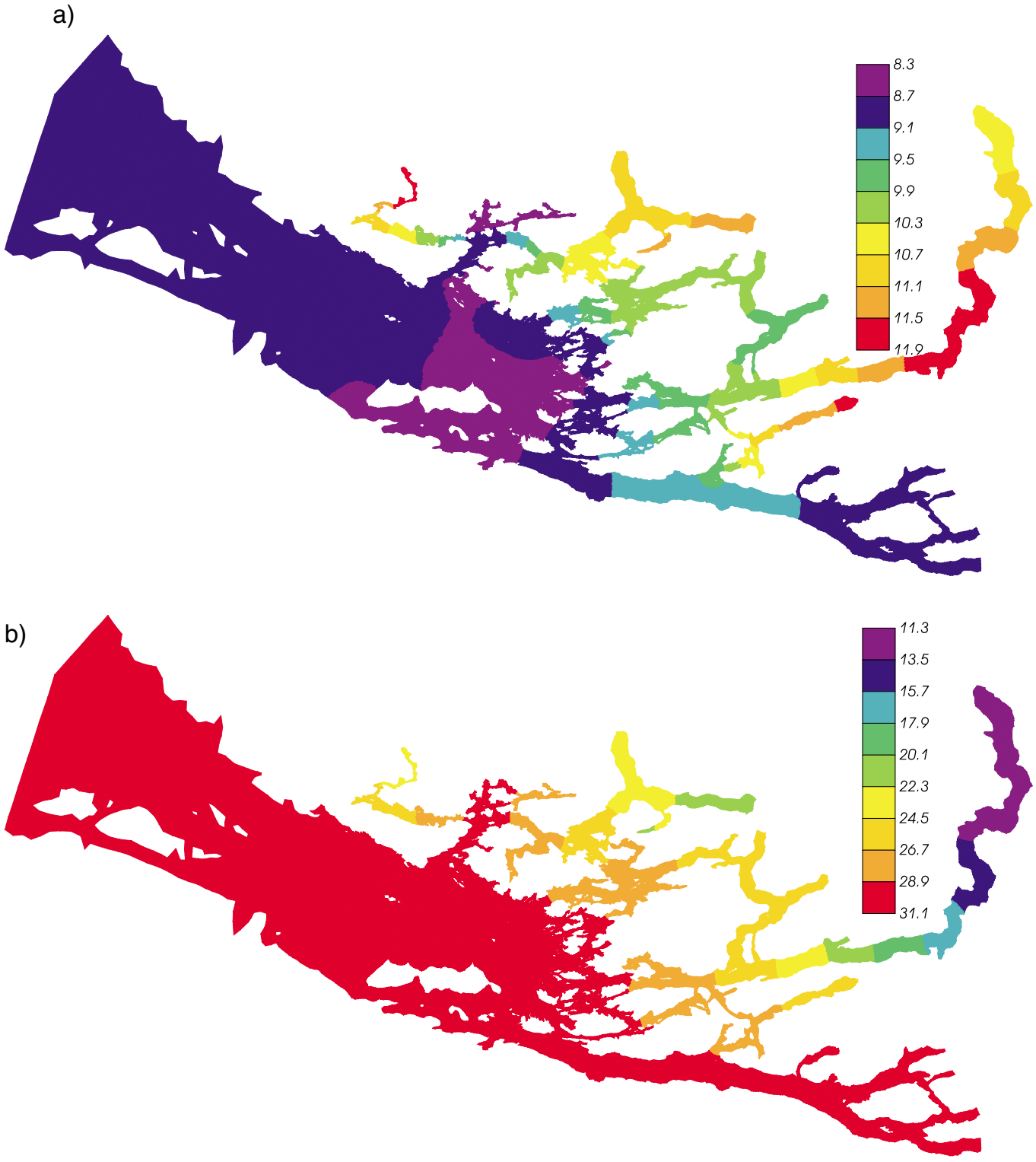

Fig. 6 Smoothed, average spring, surface a) temperatures (°C) and b) salinities (psu).

magnitude of the subtidal elevations in Penphrase Passage and Knight Inlet. These in turn are determined by the magnitudes and buoyancy of the respective discharges from the Klinaklini, Kingcome, and Wakeman rivers and mixing of the estuarine flows along the channels. Model experiments (not shown) suggest that weaker, less buoyant flows in Knight Inlet cause elevations at the confluence with Tribune Channel to be lower than those in Penphrase Passage and the surface outflow to reverse in Tribune Channel. On the other hand, larger, more buoyant estuarine flows in Knight Inlet and

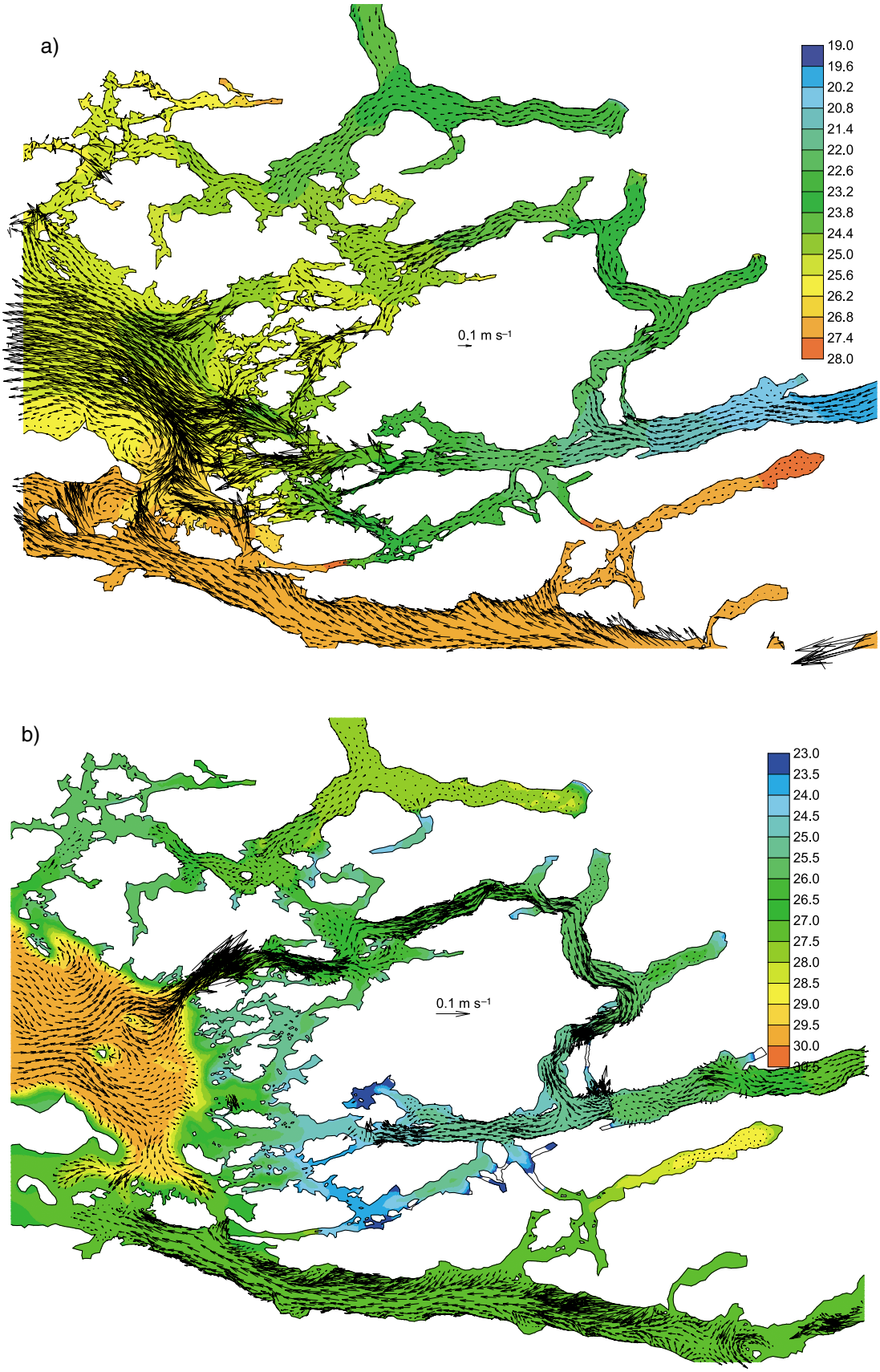

Fig. 7 Low-pass filtered salinity field and flows at a) 4 m, and b) 80 m on the last day of a fifty-day ELCIRC simulation. Only vectors at nodes separated by a minimum of 400 m are shown in a).

TABLE 1. Observed and calculated along-channel mean (Z0) current magnitudes (cm s^{-1}) and directions (degrees, counterclockwise from east) at the numbered sites (triangles) shown in Fig. 1. Time series lengths are in days. All the Johnstone Strait values are taken from TH80 while the Protection Point values are from Baker and Pond (1995). Where possible, the observed mean currents are restricted to the spring (April – June).

				Observed		ELCIRC	
No.	Site	Length	Depth (m)	Mag	Dir	Mag	Dir
10	Outer QCS (EP01S)	90	11	9.0	189	25.5	131
10	Outer QCS (EP01S)	89	52	1.5	175	3.2	299
10	Outer QCS (EP01S)	89	79	5.2	35	6.0	323
11	Q01	44	15	10.7	163	12.1	150
11	Q01	44	75	1.9	256	1.0	246
12	Q02	44	40	3.2	315	6.6	146
12	Q02	44	75	7.3	314	1.5	243
13	Fife Sound	39	5	8.9	194	7.4	191
13	Fife Sound	39	7	7.7	181	6.8	190
13	Fife Sound	39	11	5.8	174	5.5	189
13	Fife Sound	39	15	4.0	165	4.2	187
13	Fife Sound	39	19	2.7	138	3.0	185
13	Fife Sound	39	23	2.8	91	1.7	152
13	Fife Sound	39	27	3.9	60	0.4	120
13	Fife Sound	39	31	5.4	43	1.1	87
13	Fife Sound	39	35	6.9	33	1.8	55
13	Fife Sound	39	39	8.3	26	2.4	22
13	Fife Sound	91	90	11.4	8	4.2	4
13	Fife Sound	91	150	2.9	45	4.9	354
13	Fife Sound	40	210	5.8	124	0.0	0
14	Tribune Channel	39	4.5	14.4	189	7.4	191
14	Tribune Channel	39	10	15.2	190	5.5	189
14	Tribune Channel	39	15	11.7	193	4.0	187
14	Tribune Channel	39	20	9.0	194	2.8	185
14	Tribune Channel	39	25	6.3	192	1.1	138
14	Tribune Channel	39	30	4.3	193	0.9	90
14	Tribune Channel	39	35	1.9	193	1.9	47
14	Tribune Channel	39	40	0.1	299	0.4	120
14	Tribune Channel	39	90	6.3	0	4.7	15
14	Tribune Channel	39	150	0.4	32	0.0	0
15	Weynton Passage	39	8	11.7	27	22.1	66
16	Protection Point	37	2	14.2	177	11.1	168
16	Protection Point	37	9	4.9	93	7.0	164
16	Protection Point	37	12	5.7	104	5.5	160
17	Johnstone Strait 06	62	20	22.9	181	12.4	169
17	Johnstone Strait 06	62	225	9.5	351	0.7	130
18	Johnstone Strait 03	64	15	23.8	176	20.1	162
18	Johnstone Strait 03	61	150	13.3	338	1.0	350
18	Johnstone Strait 03	61	250	19.5	354	1.0	19

weaker flows in Penphrase Passage cause higher elevations to the south and more diversion of the westerly Knight Inlet flow into Tribune Channel. It has been suggested (Brent Hargreaves, personal communication, 2004; Krkošek et al., 2005) that the Knight Inlet surface estuarine flow plays a significant role in the seaward migration route of juvenile wild salmon and, in particular, which aquaculture sites these salmon pass. Thus, it is important to determine the precise conditions under which the Tribune Channel bifurcation grows or weakens. Two current meter moorings, one in Tribune Channel downstream of the confluence with Knight Inlet and another further upstream in Knight Inlet, are planned. But until this is done and the time series analysed, our preliminary numerical investigations on the dynamics underlying this bifurcation will have to suffice.

The ELCIRC estuarine flow at 80-m depth is illustrated in Fig. 7b and the flows at several depths are compared with available current meter measurements in Table 1. In particular, the 80-m flows show that the main conduit for bottom water intrusions into the archipelago is through Fife Sound and Tribune Channel, consistent with our observations (Table 1), rather than directly up Knight Inlet. This "back-door" route might be expected given the relatively shallow bathymetry at the entrance to Knight Inlet (approximately 60 m) and the much larger depths in Fife Sound and Tribune Channel (Fig. 2). Also notice the up-inlet flows in Kingcome Inlet and the eastward flows moving from Queen Charlotte Strait into Weynton Passage and then into Johnstone Strait where they go under the strong westward flows shown in Fig. 7a. However, plots from further down the water column (e.g., at 150 m) show only a weak eastward flow in Johnstone Strait, consistent with the model values given in Table 1. Therefore the flow from Queen Charlotte Strait is either insufficiently strong, or there is too much numerical dissipation in the narrow passages to produce the bottom estuarine flows reported in TH80.

Though the flow moving up Tribune Channel seems to disappear shortly after turning eastward into Knight Inlet, it only moves slightly up the water column. A similar plot at 40 m (not shown) has a continuous stream moving up both Tribune

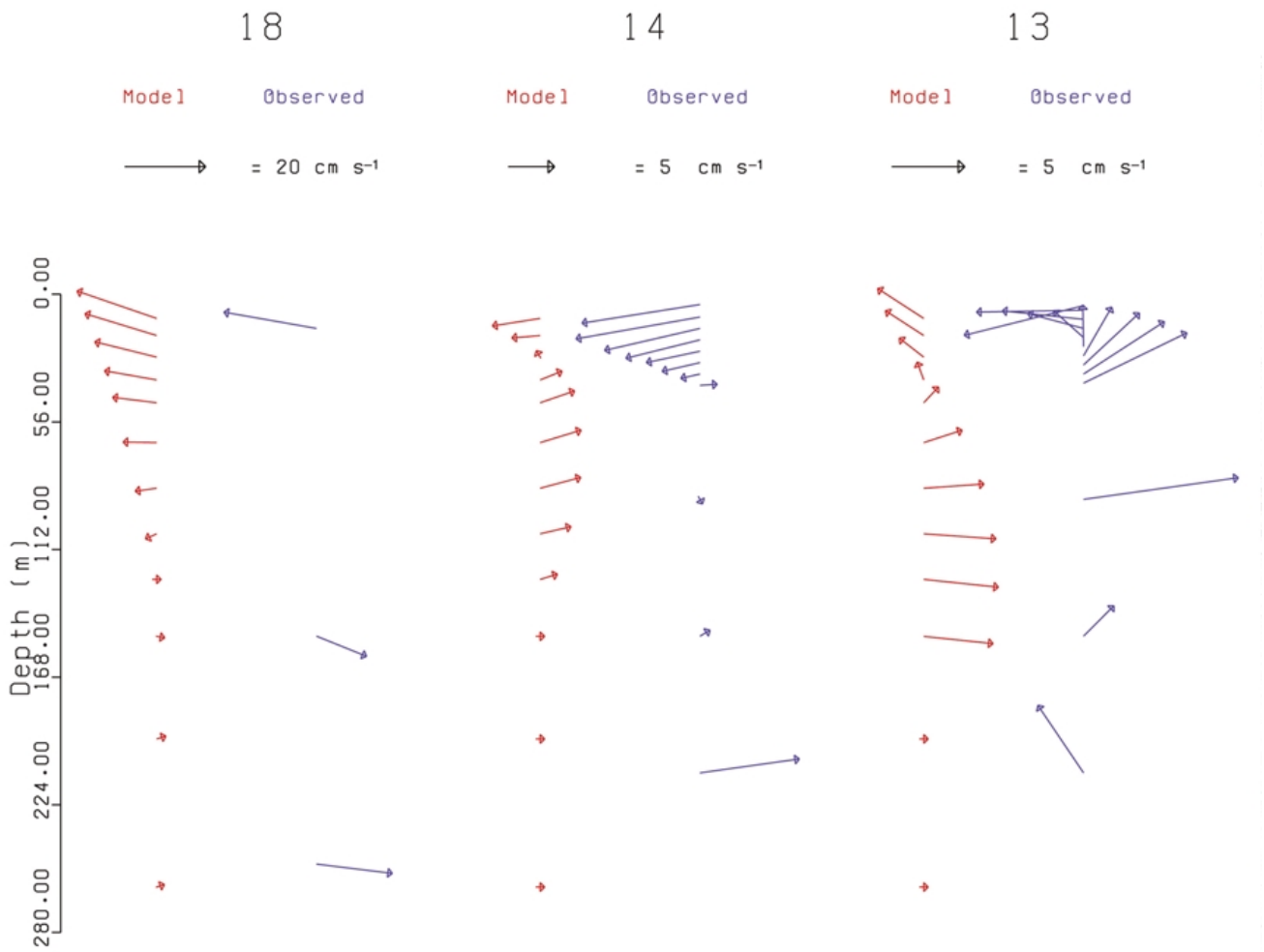

Fig. 8 Vertical profiles of observed versus ELCIRC modelled mean flows at the Johnstone Strait, Tribune Channel, and Fife Sound moorings. These are sites 18, 14, and 13, respectively, in Fig. 1.

Channel and Knight Inlet consistent with the observations of Pickard and Rogers (1959). In fact, vertical profiles of the mean flows at Protection Point (site 13 in Fig. 1) suggest that there are three flow layers in Knight Inlet, up-inlet flow between approximately 25 m and 95 m and down-inlet flow outside that range. The sub-surface flows moving water from Queen Charlotte Strait into Fife Sound and Tribune Channel play an important role in the transport of dissolved oxygen to aquaculture sites. Although beyond the scope of the present study, further investigations to examine seasonal episodes of low levels of dissolved oxygen at several sites (Stolt Sea Farms, personal communication, 2004) are clearly warranted.

Figure 8 compares observed mean (Z0) vertical profiles at mooring sites 18, 14 and 13 (Fig. 1) with their ELCIRC counterparts. The same information is also found in Table 1. Only the moorings at sites 13 and 14 were deployed as part of this study and each was comprised of an upward-looking RD Instruments Acoustic Doppler Current Profiler (ADCP) moored at 40-m depth and conventional Aanderaa RCM4 current meters further down the water column. Analysis results at all other locations were taken either from publications or harmonic analyses of archived time series.

Whereas the ELCIRC values shown in Fig. 8 indicate weak two-layer flows at all three sites, all profiles indicate too much damping, particularly near the bottom. Although the site 18 (J03) ELCIRC values near the surface have acceptable accuracy and the upper layer thickness (the depth at which the flow switches from westward to eastward) of about 120 m is close to the 100-m value given in TH80, the bottom layer values are much too weak. The ELCIRC values at both the Tribune Channel (site 14) and Fife Sound (site 13) moorings are not only seen to be weak by a factor of two near the surface, but in both cases the upper layer thicknesses are not quite right and the bottom layer flows are much too weak. These model current magnitudes and layer thicknesses are largely determined by the river and boundary discharge magnitudes, temperatures, and

TABLE 2. Observed and calculated a) M_2 and b) K_1 elevation amplitudes (cm) and phase lags (degrees, UTC) at the numbered sites (circles) shown in Fig. 1. Differences, *D* (cm), are calculated using Eq. (1).

		M_2 Obs		TIDE3D			ELCIRC		
No.	site	amplitude	phase	amplitude	phase	D	amplitude	phase	D
1	Fox Islands	123.6	250	124.1	250	0.5	124.4	250	0.8
2	Walker Group	126.7	253	127.9	251	3.3	130.6	254	4.6
3	Port Hardy	133.2	253	131.2	252	3.5	133.6	258	10.3
4	Alert Bay	127.2	260	130.8	257	6.6	137.4	263	13.5
5	Cedar Island	137.0	258	132.3	256	7.4	140.2	264	13.9
6	Montagu Point	152.7	262	146.6	257	13.6	158.2	282	54.9
7	Siwash Bay	156.2	265	152.1	257	22.1	167.8	285	55.1
8	TGN	120.9	269	119.3	267	4.4	122.4	271	5.2
9	Yorke Island	117.1	272	115.1	272	2.1	118.6	273	3.4
		K_1 Obs		TIDE3D			ELCIRC		
No.	site	amplitude	phase	amplitude	phase	D	amplitude	phase	D
1	Fox Islands	46.8	252	46.1	251	0.7	45.9	253	1.4
2	Walker Group	47.4	251	47.2	250	0.4	47.3	254	2.5
3	Port Hardy	49.9	251	48.5	251	1.3	48.3	255	4.5
4	Alert Bay	51.6	256	51.4	254	2.4	50.8	258	1.6
5	Cedar Island	51.4	253	50.3	254	1.3	50.2	258	4.9
6	Montagu Point	52.5	255	51.2	254	0.3	51.5	268	12.0
7	Siwash Bay	52.6	257	52.7	254	1.9	52.5	269	11.0
8	TGN	55.0	259	55.2	259	0.4	55.9	261	2.1
9	Yorke Island	55.8	260	57.2	261	1.8	57.0	261	1.4

salinities. Given the uncertainties in the values that were used in the model, it should not be surprising that ELCIRC has not done better. Clearly, direct rather than inferred information on the magnitude and temperature of other river discharges in the system is needed. Though some adjustments could be made to provide better near-surface agreement, experiments with a variety of mixing formulations (Mellor and Yamada, 1982; Pacanowski and Philander, 1981) and a higher resolution in the vertical had little impact on the weak sub-surface flows. In all likelihood, the interpolations associated with the Eulerian-Lagrangian time stepping have introduced too much numerical dispersion into the ELCIRC calculations.

Table 2 compares model and observed elevation harmonics at the tide gauge locations shown in Fig. 1. Average *D* values for TIDE3D over all nine sites are 7.1 and 1.2 cm for M_2 and K_1, respectively, while for ELCIRC they are 18.0 and 4.6 cm. In general, S_2 exhibited relative accuracy similar to M_2, while O_1 had a relative accuracy similar to K_1. Though only barotropic, TIDE3D was clearly much more accurate. For both models, the K_1 elevation harmonics are seen to be closer to their tide gauge counterparts than M_2. The largest M_2 discrepancies are in Knight Inlet where for ELCIRC, the amplitudes are too large and the phases are too late (large), while for TIDE3D they are too small and too soon. In both cases (though to different degrees), we suspect that these errors arise from a combination of inaccurate numerics, inaccurate bathymetry, and missing physics. For example, when TIDE3D is rerun with the same smoothed bathymetry as ELCIRC, the M_2 phase lags at Montagu Point and Siwash Bay increase to 269° and 274° respectively. This indicates that the shallower smoothed depths have retarded propagation up the inlet by at least 12° and partially explains the late M_2 phases arising in the ELCIRC simulation.

Table 3 compares model and observed ellipse parameters at the current mooring locations also shown in Fig. 1. In order to be consistent with the spring initial conditions and river discharges, when possible these parameters were computed for only that portion of the time series within the April to June time period. As all current meter locations are in relatively narrow channels where the flow is generally rectilinear, only the along-channel speeds and phase lags are used in the comparison. The presence of internal tides and other baroclinic effects means that there is generally less agreement here than with the tidal elevations. Nevertheless, at all sites except Weynton Passage where a factor of two discrepancy in the M_2 speed seems suspicious, the barotropic TIDE3D simulation has provided reasonably accurate benchmark values against which the baroclinic model can be gauged.

Figure 9 also gives a graphical presentation of the model versus observed comparison at the Johnstone Strait and Fife Sound moorings. Though the M_2 ELCIRC near-surface speeds at J03 are quite accurate (Fig. 9a), the associated phases are too late by approximately one hour. Further down the water column, the model current ellipses have not captured the baroclinity seen in the observations. The same is generally true for K_1, although in this case the model phases are too soon by approximately five hours near the surface and three hours at depth. In both cases, the model profiles show too much damping and earlier arrival times with depth. The comparisons at Fife Sound (Fig. 9b) are equally unsatisfactory. Although the phases are reasonably accurate, the near-surface speeds are too large (especially for M_2) while those near the bottom are too small. Despite the potential for capturing the baroclinic effects seen in the observations, it generally appears that the ELCIRC simulated tides are no more (and

TABLE 3. Observed and calculated along-channel a) M_2 and b) K_1 current amplitudes (cm s^{-1}) and phase lags (degrees, UTC) at the numbered sites (triangles) shown in Fig. 1.

a)			Obs.		TIDE3D		ELCIRC	
No.	site	depth (m)	amplitude	phase	amplitude	phase	amplitude	phase
10	Outer QCS (EP01)	11	17.4	353	17.7	36	37.6	22
10	Outer QCS (EP01)	52	20.9	11	17.5	34	32.3	16
10	Outer QCS (EP01)	79	29.5	24	16.9	32	20.1	8
11	Q01	15	23.7	36	11.1	43	24.3	17
11	Q01	75	16.7	43	11.3	41	16.5	12
12	Q02	40	19.0	42	10.2	46	22.1	27
12	Q02	75	12.1	21	10.2	46	20.0	18
13	Fife Sound	5	17.6	359	13.8	358	46.0	24
13	Fife Sound	7	19.5	10	13.8	358	45.7	23
13	Fife Sound	11	20.3	23	13.8	358	45.1	22
13	Fife Sound	15	20.1	33	13.8	358	44.6	21
13	Fife Sound	19	19.8	40	13.8	358	44.0	20
13	Fife Sound	23	19.5	44	13.8	358	43.3	19
13	Fife Sound	27	20.1	48	13.8	358	42.7	18
13	Fife Sound	31	20.1	51	13.8	358	42.3	18
13	Fife Sound	35	20.0	53	13.8	358	41.9	17
13	Fife Sound	39	19.4	54	13.8	358	41.4	16
13	Fife Sound	90	15.5	48	13.8	358	30.8	8
13	Fife Sound	150	21.9	6	14.0	358	13.9	359
13	Fife Sound	210	30.6	351	13.9	356	6.4	0
14	Tribune Channel	4.5	28.7	174	18.8	187	37.7	208
14	Tribune Channel	10	29.2	196	18.8	187	37.9	208
14	Tribune Channel	15	28.1	199	18.8	187	38.0	207
14	Tribune Channel	20	27.1	199	18.8	187	38.1	207
14	Tribune Channel	25	26.9	197	18.8	187	38.3	205
14	Tribune Channel	30	25.9	196	18.8	187	38.3	204
14	Tribune Channel	35	24.9	195	18.8	187	38.3	202
14	Tribune Channel	40	23.9	194	18.8	187	38.3	200
14	Tribune Channel	90	19.4	196	19.0	187	24.1	184
14	Tribune Channel	150	11.9	176	19.1	184	6.1	155
15	Weynton Passage	8	163.6	83	72.3	112	61.0	80
16	Protection Point	2	13.4	202	17.5	170	41.5	217
16	Protection Point	9	1.7	346	17.5	170	40.5	216
16	Protection Point	12	14.1	191	17.5	170	40.1	216
17	Johnstone Strait 06	20	30.3	84	32.5	109	27.8	104
17	Johnstone Strait 06	225	22.7	95	33.8	108	7.2	70
18	Johnstone Strait 03	15	25.6	92	42.0	111	25.5	120
18	Johnstone Strait 03	150	40.4	97	43.3	110	15.2	78
18	Johnstone Strait 03	250	46.9	92	41.8	106	6.2	58

b)			Obs.		TIDE3D		ELCIRC	
No.	site	depth (cm)	amplitude	phase	amplitude	phase	amplitude	phase
10	Outer QCS (EP01)	11	6.9	328	8.5	16	9.1	2
10	Outer QCS (EP01)	52	6.4	341	8.5	18	8.0	344
10	Outer QCS (EP01)	79	8.9	351	8.5	22	4.8	336
11	Q01	15	4.0	356	7.3	5	5.3	351
11	Q01	75	6.2	352	7.5	6	3.8	337
12	Q02	40	4.5	348	6.5	10	5.3	347
12	Q02	75	3.3	347	6.5	10	5.0	345
13	Fife Sound	5	8.6	316	3.8	352	10.9	8
13	Fife Sound	7	9.8	324	3.8	352	10.7	7
13	Fife Sound	11	10.0	332	3.8	352	10.3	6
13	Fife Sound	15	10.2	342	3.8	352	10.0	5
13	Fife Sound	19	10.6	351	3.8	352	9.6	4
13	Fife Sound	23	11.3	359	3.8	352	9.3	3
13	Fife Sound	27	12.2	2	3.8	352	9.0	2
13	Fife Sound	31	12.6	5	3.8	352	8.8	2
13	Fife Sound	35	12.8	6	3.8	352	8.6	2
13	Fife Sound	39	12.9	7	3.8	352	8.4	2
13	Fife Sound	90	7.6	354	3.7	351	5.3	1
13	Fife Sound	150	2.9	0	3.7	351	2.0	4
13	Fife Sound	210	1.0	319	3.6	358	0.9	8
14	Tribune Channel	4.5	9.2	207	4.6	173	7.6	191
14	Tribune Channel	10	7.3	201	4.6	183	7.6	191
14	Tribune Channel	15	7.2	207	4.6	173	7.5	190
14	Tribune Channel	20	7.0	213	4.6	173	7.5	189
14	Tribune Channel	25	6.3	214	4.6	173	7.3	187

Table 3. *Continued*

			Obs.		TIDE3D		ELCIRC	
No.	site	depth (cm)	amplitude	phase	amplitude	phase	amplitude	phase
14	Tribune Channel	30	5.8	216	4.6	173	7.3	186
14	Tribune Channel	35	5.4	216	4.6	173	7.1	184
14	Tribune Channel	40	4.3	214	4.6	173	7.0	183
14	Tribune Channel	90	2.5	168	4.6	172	3.8	166
14	Tribune Channel	150	4.5	154	4.7	175	0.8	145
15	Weynton Passage	8	48.3	348	50.5	50	21.7	327
16	Protection Point	2	6.6	260	3.2	162	7.6	190
16	Protection Point	9	1.6	212	3.2	162	7.6	191
16	Protection point	12	5.2	238	3.2	162	7.6	191
17	Johnstone Strait 06	20	2.0	316	14.0	26	8.3	313
17	Johnstone Strait 06	225	9.6	353	14.4	25	1.7	290
18	Johnstone Strait 03	15	9.8	36	17.1	24	8.9	313
18	Johnstone Strait 03	150	13.9	343	17.7	25	3.1	286
18	Johnstone Strait 03	250	16.3	320	17.5	31	1.0	266

perhaps even less) accurate than those obtained with TIDE3D. An inspection of the salinity time series at Protection Point (site 16 in Fig. 1) reveals M_2 oscillations of 0.55 ppt at 5-m depth. Although, these oscillations may, in part, be due to the presence of internal tides, the surface temperature gradients in this region (Fig. 6b) indicate that the oscillations could also be explained by horizontal advection associated with barotropic tidal currents. Indeed, the poor representation of the baroclinic tidal currents at J03 and Fife Sound casts doubt on the likelihood that similar features would be accurately represented in Knight Inlet. Unfortunately, all current meter observations taken during the extensive Institute of Ocean Sciences (IOS) studies in the 1970s and 1980s (e.g., Freeland and Farmer, 1980) seem to have been lost and thus cannot be used for further model evaluation. Furthermore, as noted previously, Stacey et al. (1995) had to augment the standard Mellor-Yamada vertical diffusion coefficients (Mellor and Yamada, 1982) by an extra term in order to represent the mixing caused by breaking internal waves in this region. The fact that this has not been done here would be expected to contribute further to ELCIRC inaccuracies in representing the internal tides in Knight Inlet. A final important factor in accurately simulating internal tides is that the density field in the model be representative of the time period of the current observations. Clearly, the sparsity of our CTD observations restricted the degree to which this was possible.

Although beyond the scope of the present study we also note that there are several bottlenecks within the model domain, such as Weynton Passage and the Knight Inlet sill, where the spring/neap tidal modulation can be expected to provide a fortnightly pulsing of the subtidal estuarine flows. This phenomenon has been studied before in Knight Inlet by Stacey et al. (1995) and in Juan de Fuca Strait and the Strait of Georgia by Griffith and LeBlond (1990) and Masson (2002), respectively. Clearly it warrants further examination. In particular, as Weynton Passage is only about 90 m deep, there must be very strong shears (and mixing) between the incoming and outgoing 30,000 $m^3\ s^{-1}$ estuarine flows that were estimated further westward in Johnstone Strait by TH80.

4 Summary and conclusions

We have described the use of CTD and current meter observations and the application of two models to understand better the average spring circulation in the Broughton Archipelago, the primary location for salmon farms in British Columbia. Although the TIDE3D model is only barotropic, it was able to simulate the tidal elevations and 3D tidal flows with reasonable accuracy. It also predicted the existence of tidal residual eddies in eastern Queen Charlotte Sound and the channel north of Alert Bay, features that were partially obscured by (but still evident in) the strong estuarine flows computed by ELCIRC. (However, there is no observational evidence to support the existence of these eddies.) Theoretically, ELCIRC should have been able to simulate the baroclinic components of the tide as well as the strong estuarine background flows that are largely determined by river discharge. However, we found substantial inaccuracies in the model representation of these features. Largely due to its lower order numerical approximations and an overly diffusive Lagrangian approach to the calculation of the material derivatives, ELCIRC was seen to be much too dispersive. This was clearly evident in the model versus measured vertical profiles of both the mean background flows and the M_2 and K_1 tidal ellipses at two representative moorings in the archipelago.

Though there are presently no observations for confirmation, the ELCIRC results suggest that Tribune Channel plays a much larger role than previously suspected in linking the circulations of the Broughton Archipelago and Knight Inlet. The relative magnitude of the surface estuarine flow turning the corner from Knight Inlet and entering Tribune Channel seems to be governed by the surface elevation difference between Knight Inlet and Penphrase Passage. Higher values in Knight Inlet cause higher diversions into Tribune Channel. These elevation differences arise from the relative magnitudes of the two estuarine flows and their dynamic heights. Furthermore, the bottom estuarine flow in Knight Inlet seems to arise from flows up Fife Sound and Tribune Channel, rather than directly from the mouth of Knight Inlet. Both these results have important ramifications for the Broughton Archipelago aquaculture industry. The bottom flows can be

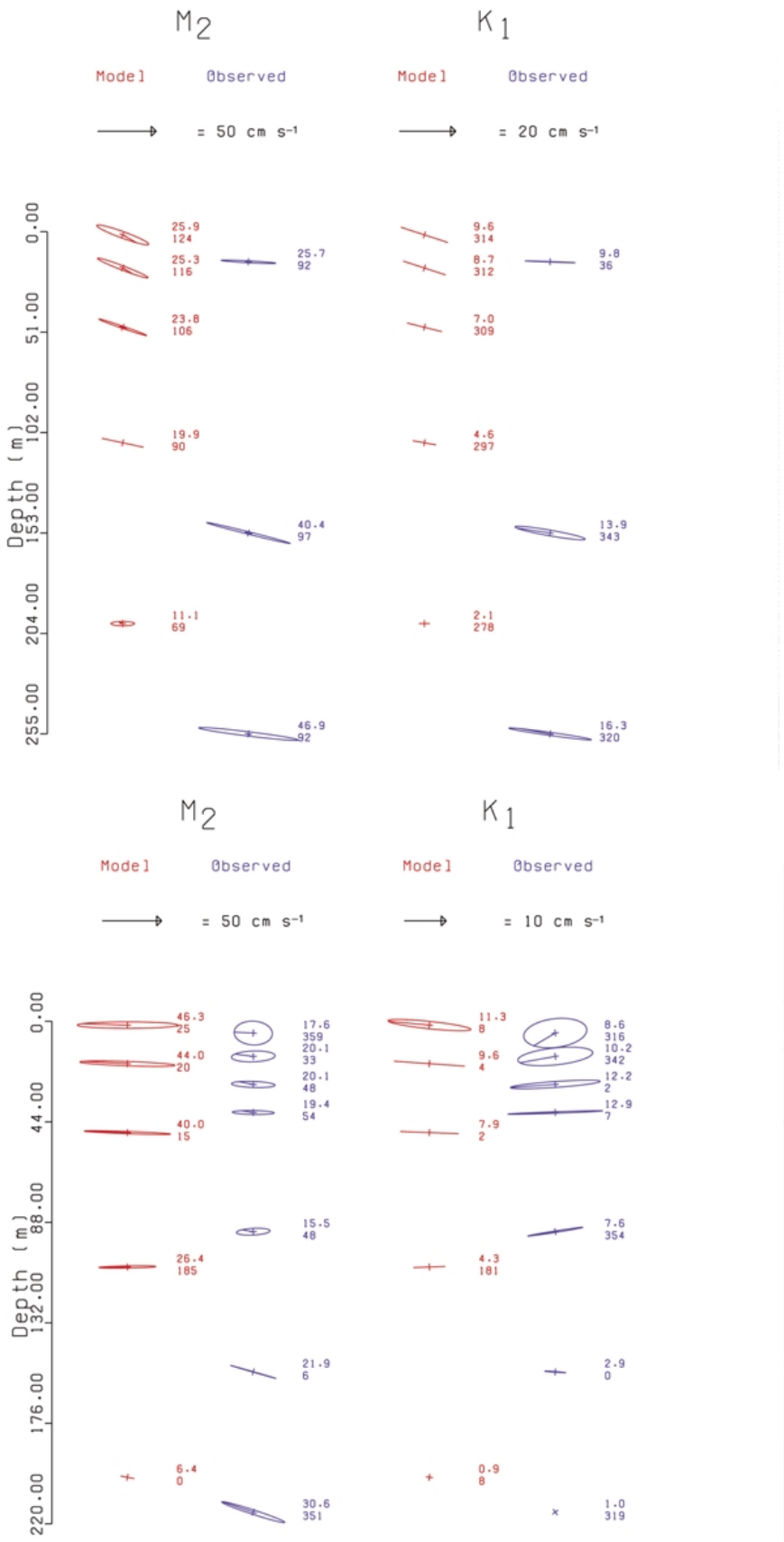

Fig. 9 a) Johnstone Strait (J03) and b) Fife Sound M_2 and K_1 tidal ellipses from harmonic analysis of observational time series and the last ten days of a fifty-day ELCIRC simulation. Only every third level is shown for the model results.

expected to play an important role in providing dissolved oxygen to the salmon farms while the surface flows, to a large extent, determine the seaward migration corridor for juvenile salmon originating in upper Knight Inlet and the likely transport route for buoyant organisms within the archipelago. Consequently, these surface flows can be expected to have important implications for the potential interactions (e.g., transfer of sea lice and viruses) between farmed and wild salmon (Krkošek et al., 2005).

The Broughton Archipelago is a complex region with strong tidal, estuarine, and wind-driven flows. Although the preceding investigation has given a preliminary overview of the general circulation patterns, there are numerous additional studies that need to be carried out. These include examinations of the wind-driven flows, the spring/neap modulation of estuarine flows in constrictions like Weynton Passage, and flow bifurcation at important junctions such as the Knight Inlet and Tribune Channel confluence. Clearly, a less dissipative model that allows a better representation of internal tides and bottom estuarine flows is also needed. Future studies are planned to address these issues.

Acknowledgements

We thank Falconer Henry for grid creation and useful advice; Jake Galbraith for processing the CTD data; Clare Backman and Dale Blackburn of Stolt Sea Farms Inc. for helpful discussions; Trish Kimber for assistance with some of the figures; the crews of CCGS *Vector* and CCGS *John P. Tully* for assistance with the field studies; two anonymous reviewers for their constructive comments on an earlier version of this paper; and the Aquaculture Collaborative Research and Development Program (ACRDP-Project number P-01-09-005) for partial financial support.

References

BAKER, P. and S. POND. 1995. The low-frequency residual circulation in Knight Inlet, British Columbia. *J. Phys. Oceanogr.* **25**: 747–763.

BAPTISTA, A.M.; Y. ZHANG, A. CHAWLA, M. ZULAUF, C. SEATON, E.P. MYERS III, J. KINDLE, M. WILKIN, M. BURLA and P.J. TURNER. 2005. A cross-scale model for 3D baroclinic circulation in estuary-plume-shelf systems: II. Application to the Columbia River. *Continental Shelf Res.* **25**: 935–972.

CASULLI, V. and R.A. WALTERS. 2000. An unstructured grid, three-dimensional model based on the shallow water equations. *Int. J. Numerical Methods in Fluids*, **32**: 331–348.

CENTER FOR COASTAL AND LAND-MARGIN RESEARCH. 2004. About CCALMR. Available from http://www.ccalmr.ogi.edu/about-ccalmr.html.

DI LORENZO, E.; M.G.G. FOREMAN and W.R. CRAWFORD. 2005. Modelling the generation of Haida Eddies. *Deep Sea Res. II*, **52**: 853–873.

HYDAT CD-ROM, 1999. Surface water and sediment data, version 96-1.04. Water Survey of Canada, Environment Canada, Atmospheric Environment Program.

FARMER, D.M. and J.D. SMITH. 1980a. Tidal interaction of stratified flow with a sill in Knight Inlet. *Deep-Sea Res.* **27A**: 239–254.

—— and ——. 1980b. Generation of lee waves over the sill in Knight Inlet. In: *Fjord Oceanography.* H.J. Freeland, D.M. Farmer and C.D. Levings (Eds.), Plenum Press, pp 259–269.

—— and H.J. FREELAND. 1983. The physical oceanography of fjords. *Prog. Oceanogr.* **12**: 147–219.

FOREMAN, M.G.G. and R.F. HENRY. 1989. The harmonic analysis of tidal model times series. *Adv. Water Resour.* **12**: 109–120.

——; ——, R. A. WALTERS and V. A. BALLANTYNE. 1993. A finite element model for tides and resonance along the north coast of British Columbia. *J. Geophys. Res. Oceans, C2,* **98**: 2509–2531.

——; R.A. WALTERS, R.F. HENRY, C.P. KELLER and A.G. DOLLING. 1995. A tidal model for eastern Juan de Fuca Strait and the southern Strait of Georgia. *J. Geophys. Res. Oceans, C1*, **100**: 721–740.

—— and R.E. THOMSON. 1997. Three-dimensional model simulations of tides and buoyancy currents along the west coast of Vancouver Island. *J. Phys. Oceanogr.* **27**(7): 1300–1325.

——; G. SUTHERLAND and P.F. CUMMINS. 2004. Tidal dissipation around Vancouver Island: An inverse approach. *Continental Shelf Res.* **24**: 2167–2185.

FREELAND, H.J. and D. FARMER. 1980. Circulation and energetics of a deep, strongly stratified inlet. *Can. J. Fish. Aquat. Sci.* **37**: 1398–1410.

GOLDEN SOFTWARE, INC. 2004. Surfer. Available from http://www.goldensoftware.com/products/surfer/surfer.shtml.

GRIFFITH, D.A. and P.H. LEBLOND. 1990. Estuary/ocean exchange controlled by spring-neap tidal mixing. *Estuarine Coastal Shelf Sci.* **30**: 275–297.

HANEY, R.L. 1991. On the pressure gradient force over steep topography in sigma coordinate ocean models. *J. Phys. Oceanogr.* **21**: 610–619.

HANNAH, C.G. and D.G. WRIGHT. 1995. Depth dependent analytical and numerical solutions for wind driven flow in the coastal ocean. In: *Quantitative Skill Assessment for Coastal Ocean Models, Coastal and Estuarine Ser.*, Vol. 47, D.R. Lynch and A.M Davies (Eds) AGU, Washington, D.C. pp. 125–152,

HENRY, R.F. and R.A. WALTERS. 1993. A geometrically-based, automatic generator for irregular triangular networks. *Commun. Numer. Methods Eng.* **9**: 555–566.

KRKOŠEK, M.; M.A. LEWIS and J.P. VOLPE. 2005. Transmission dynamics of parasitic sea lice from farm to wild salmon. *In*: Proc. Royal Society B, doi:10.1098/rspb.2004.3027.

LYNCH, D.R.; J.T. IP, C.E. NAIMIE and F.R. WERNER. 1996. Comprehensive coastal circulation model with application to the Gulf of Maine. *Continental Shelf Res.* **16**(7): 875–906.

MARSDEN, R.F. and K.C. GREENWOOD. 1994. Internal tides observed by an acoustic Doppler current profiler, *J. Phys. Oceanogr.* **24(6)**: 1097–1109.

MASSON, D. 2002. Deep water renewal in the Strait of Georgia. *Estuarine Coastal Shelf Sci.* **54**: 115–126.

MELLOR, G.L. and T. YAMADA. 1982. Development of turbulence closure model for geophysical fluid problems. *Rev. Geophysics*. **20**: 851–875.

——; T. EZER and L.-T. OEY. 1994. The pressure gradient conundrum of sigma coordinate ocean models. *J. Atmos. Ocean. Technol.* **11**: 1126–1134.

PACANOWSKI, R.C. and S.G.H. PHILANDER. 1981. Parameterization of vertical mixing in numerical models of tropical oceans. *J. Phys. Oceanogr.* **11**: 1443–1451.

PICKARD, G.L. and K. ROGERS. 1959. Current measurements in Knight Inlet, British Columbia. *J. Fish. Res. Board Can*. **16**: 635–678.

ROBINSON, C.L.K.; J. MORRISON, and M.G.G. FOREMAN. 2005. Oceanographic connectivity among marine protected areas on Canada's northern Pacific coast. *Can. J. Fish. Aquat. Sci.* **62**: 1350–1362.

STACEY, M.W.; S. POND and Z.P. NOWAK. 1995. A numerical model of the circulation in Knight Inlet, British Columbia, Canada. *J. Phys. Oceanogr.* **24**: 1037–1062.

STATISTICS CANADA. 2005. Table 003–0001, Aquaculture, production and value, annual (290 series), available from http://cansim2.statcan.ca/cgi-win/CNSMCGI.EXE?Lang=E&ArrayId=003-0001&Array_Pick=1&Detail=1&ResultTemplate=CII/CII___&RootDir=CII/

THOMSON, R.E. and W.S. HUGGETT. 1980. M_2 baroclinic tides in Johnstone Strait, British Columbia. *J. Phys. Oceanogr.* **10**: 1509–1539.

UMLAUF, L. and J. BURCHARD. 2003. A generic length-scale equation for geophysical turbulence models. *J. Mar. Res*. **6(12)**: 235–265.

WALTERS, R.A. 1988. A finite element model for tides and currents with field applications. *Commun. Appl. Numer. Meth.* **4**: 401–411.

——. 1992. A three-dimensional, finite element model for coastal and estuarine circulation. *Continental Shelf Res*. **12**: 83–102.

——; D.G. GORING and R.G. BELL. 2001. Ocean tides around New Zealand. *New Zealand J. Mar. Freshwater Res.* **35**: 567–579.

WEBB, A.J. and S. POND. 1986. A modal decomposition of the internal tide in a deep, strongly stratified inlet: Knight Inlet, British Columbia. *J. Geophys. Res*. **91**: 9721–9738.

ZHANG, Y.; A.M. BAPTISTA and E.P. MYERS. 2004. A cross-scale model for 3D baroclinic circulation in estuary-plume-shelf systems: I. Formulation and skill assessment. *Continental Shelf Res.* **24(18)**: 2187–2214.